



HAL
open science

Highly dispersed silica-supported iridium and iridium–aluminium catalysts for methane activation prepared via surface organometallic chemistry

Léon Escomel, Daniel Abbott, Victor Mougel, Laurent Veyre, Chloé Thieuleux, Clément Camp

► To cite this version:

Léon Escomel, Daniel Abbott, Victor Mougel, Laurent Veyre, Chloé Thieuleux, et al.. Highly dispersed silica-supported iridium and iridium–aluminium catalysts for methane activation prepared via surface organometallic chemistry. *Chemical Communications*, 2022, 58 (59), pp.8214-8217. 10.1039/D2CC02139K . hal-03739621

HAL Id: hal-03739621

<https://hal.science/hal-03739621>

Submitted on 28 Jul 2022

HAL is a multi-disciplinary open access archive for the deposit and dissemination of scientific research documents, whether they are published or not. The documents may come from teaching and research institutions in France or abroad, or from public or private research centers.

L'archive ouverte pluridisciplinaire **HAL**, est destinée au dépôt et à la diffusion de documents scientifiques de niveau recherche, publiés ou non, émanant des établissements d'enseignement et de recherche français ou étrangers, des laboratoires publics ou privés.

COMMUNICATION

Highly Dispersed Silica-Supported Iridium and Iridium-Aluminium Catalysts for Methane Activation Prepared via Surface Organometallic Chemistry

Received 00th January 20xx,
Accepted 00th January 20xx

DOI: 10.1039/x0xx00000x

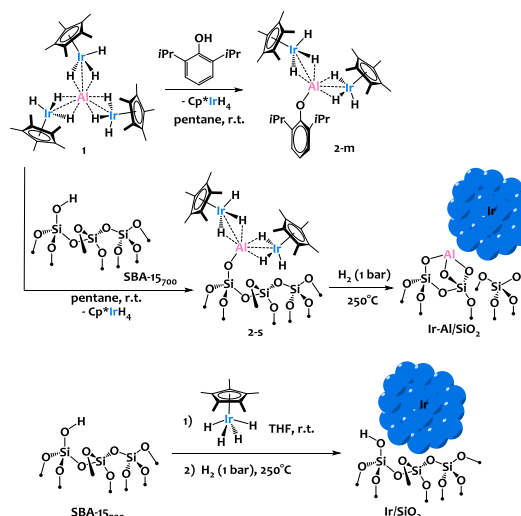
Léon Escomel,^a Daniel F. Abbott,^b Victor Mougel,^b Laurent Veyre,^a Chloé Thieuleux^a and Clément Camp*^a

The grafting of an iridium-aluminium precursor onto silica followed by thermal treatment under H₂ yields small (<2 nm), narrowly distributed nanoparticles used as catalysts for methane H/D exchange. This Ir-Al/SiO₂ catalyst demonstrated enhanced catalytic performances in comparison with the monometallic Ir/SiO₂ analogue (TOFs of 339 h⁻¹ versus 117 h⁻¹ respectively), highlighting the promoting effect of aluminium. TON up to 900 is obtained after 9 hours, without evidence of catalyst deactivation, and identical performances are achieved after air exposure, underlining the good robustness of both Ir-Al/SiO₂ and Ir/SiO₂ catalytic materials. This work opens new perspectives for the fundamental understanding of the activation of relatively inert alkane C-H bonds.

Promoters are ubiquitous in heterogeneous catalysis, and a large number of precious metal catalysts are modified by the addition of a second metal component to enhance the catalysts' activity, selectivity or robustness as compared to monometallic analogues. Methane hydrogen/deuterium (H/D) exchange is the simplest methane transformation, yet of high fundamental importance for understanding the activation of relatively inert C-H bonds, and of potential interest for labelling studies. To date, a range of transition metal films were found capable of catalytic CH₄ H/D exchange, with different efficiencies and selectivities.¹⁻³ Dehydrated aluminas are also proficient in methane deuteration⁴ via a mechanism involving heterolytic C-H bond splitting across Al-O moieties.⁵ Combining Lewis acidic Al sites with transition metals thus appears attractive for potentially promoting this transformation, yet this strategy has not been described to the best of our knowledge. Precise synthesis of systems with a homogeneous distribution of two metallic components is

challenging, yet critical for a rational understanding of structure/activity relationships. Surface Organometallic Chemistry (SOMC) is a powerful approach to address this challenge, that was used with success to generate well-defined surface organometallic fragments and highly dispersed nanoparticles (Nps) homogeneously distributed at the surface of solid supports.^{6,7} Accordingly, in recent years, attractive catalysts prepared by SOMC and containing two metal components emerged in the literature as a way to enhance activity and selectivity performances for instance in CO₂ reduction⁸⁻¹⁰ or alkane dehydrogenation.^{11,12} Our contribution to this field was the discovery of original silica-supported Ta/Ir catalysts highly active in H/D exchange reactions of arenes, and prepared from molecular heterobimetallic complexes isolated in solution.¹³⁻¹⁵

We recently described the synthesis of an original iridium-aluminium complex, [(Cp*IrH₃)₃Al], **1** (Scheme 1), and have demonstrated the lability of the [Cp*IrH₃]⁻ iridate moieties surrounding the Al(III) cation, notably in presence of protic species.¹⁶ We hypothesized that such protonolysis reactivity could be used with profit for the grafting of **1** onto silica.



Scheme 1 – SOMC approach for the preparation of Ir-Al surface species and Nps.

^a Université de Lyon, Institut de Chimie de Lyon, Laboratory of Catalysis, Polymerization, Processes & Materials, CP2M UMR 5128 CNRS-UCB Lyon 1-CPE Lyon, CPE Lyon 43 Bd du 11 Novembre 1918, F-69616 Villeurbanne, France. clement.camp@univ-lyon1.fr

^b Laboratorium für Anorganische Chemie, ETH Zürich, Vladimir-Prelog-Weg 1, CH-8093 Zürich, Switzerland

Electronic Supplementary Information (ESI) available: [Experimental, NMR, IR, XRD, STEM, EDS, XPS, chemisorption, catalysis data]. See DOI: 10.1039/x0xx00000x

To anticipate the reactivity of **1** with silica surface silanols, we first investigated the reaction of **1** with 1 equiv. of 2,6-diisopropylphenol. This yielded selectively the mono-substituted $[\text{Al}(\text{OAr})(\text{Cp}^*\text{IrH}_3)_2]$ ($\text{Ar} = 2,6\text{-}(i\text{Pr})\text{C}_6\text{H}_3$) complex, **2-m**, along with one equivalent of IrCp^*H_4 as coproduct of reaction (Scheme 1). Complex **2-m** was fully characterized (see ESI), and displayed a structure typical of Ir-Al species as previously described by our group where the iridate centers are held around the Al^{3+} cation through bridging hydrides and polarized metal-metal interactions.^{16,17} This preliminary investigation validated the proposed ligand exchange reactivity, which is facile, selective and results in the formation of a robust Al-O bond. Furthermore, **2-m** can serve as a good structural model and provides reference to decipher the spectroscopic data of the species grafted on silica (see below). We then treated mesoporous silica, namely SBA-15, dehydroxylated at 700°C (SBA-15₇₀₀)^{6,13} with a pentane solution of **1** at room temperature, leading to material **2-s** (Scheme 1). The IR spectra show the consumption of the surface isolated silanols ($\nu(\text{OH}) = 3748 \text{ cm}^{-1}$, see Figure 1-a and 1-b) and the appearance of new signals attributed to metal-hydride stretches at 2131 and 2000 cm^{-1} and $\nu(\text{C-H})$ from the Cp^* ligands at 2913-2989 cm^{-1} (Figure 1). This IR signature is similar to the IR spectrum of **2-m** (see Figure S8), which testifies to the relevance of **2-m** as molecular model for the surface species **2-s**. During the reaction, 1 equiv. of IrCp^*H_4 is formed *per* grafted Al, which is removed from the material by successive pentane washings, and quantified by $^1\text{H-NMR}$ spectroscopy (see ESI). These analyses are in agreement with the chemical grafting of the precursor onto silica *via* protonolysis of one $[\text{Cp}^*\text{IrH}_3]$ group by a surface silanol, as seen in the preparation of **2-m**, yielding the monopodal surface species $(\equiv\text{SiO})\text{Al}(\text{Cp}^*\text{IrH}_3)_2$, **2-s**. Solid-state ^1H and ^{13}C NMR spectroscopy analyses (see ESI) support the proposed structure for **2-s**, with notably a broad Ir-H resonance averaged at $\delta(^1\text{H}) = -17.14 \text{ ppm}$ (vs. -16.55 in **2-m**). The elemental analysis data for this solid (expected weight %: C 10.62, H 1.60, Ir 17.00, Al 1.19; found: C 10.87, H 1.69, Ir 16.40, Al 1.21; expected ratios: C/Al=20.0, Ir/Al=2.0; found: C/Al=20.1, Ir/Al=1.9) are also in excellent agreement with the proposed formula for **2-s** and correspond to 0.53 surface organometallic sites *per* nm^2 of silica, as expected for this type of support.^{13,14}

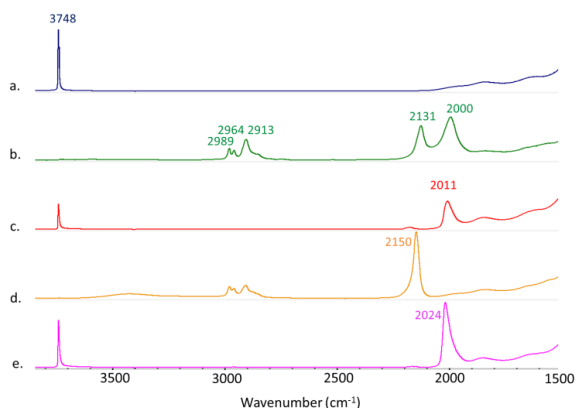


Figure 1 – Diffuse Reflectance Infrared Fourier Transform spectra of SBA-15₇₀₀ (a), $\equiv\text{SiOAl}(\text{Cp}^*\text{IrH}_3)_2$ **2-s** (b), **Ir-Al/SiO₂** (c), Cp^*IrH_4 physisorbed on SBA-15₇₀₀ (d) and **Ir/SiO₂** (e) recorded on powder materials under argon.

Next, thermal treatment of **2-s** under H_2 (1 bar, 250°C) produced material **Ir-Al/SiO₂** as a deep brown powder. The IR spectrum of **Ir-Al/SiO₂** (Figure 1-c) shows drastic changes in the Ir-H bands, with the disappearance of the signal at 2131 cm^{-1} , and a slight shift of the signal at 2000 cm^{-1} to 2011 cm^{-1} . Furthermore, the C-H stretches vanished compared to those in **2-s**, and some isolated silanols are restored ($\nu_{\text{OH}} = 3748 \text{ cm}^{-1}$). These spectral data suggest decomposition of surface species and removal of the organic Cp^* ligands. This is confirmed by elemental analysis, with low C and H weight percent (%C = 0.69 and %H = 0.24, C/Al ratio = 1.2). The Ir/Al atomic ratio of 1.9 remains unchanged, indicating that only the organic ligands are affected by the thermal treatment under H_2 . High-angle annular dark-field scanning transmission electron microscopy (HAADF-STEM) images of **Ir-Al/SiO₂** show the formation of small, narrowly distributed and well dispersed Nps at the surface of the SBA-15 support, with a mean size of $1.6 \pm 0.4 \text{ nm}$ (see Figure 2A and ESI).

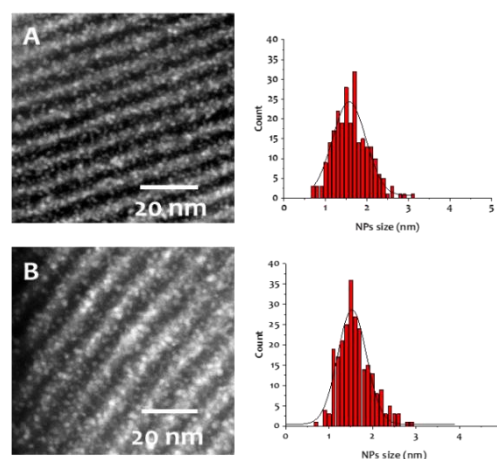


Figure 2 –STEM-HAADF micrographs and Nps size distribution of **Ir-Al/SiO₂** (A) and **Ir/SiO₂** (B) materials (bar scales: 20 nm).

EDS analyses show that Ir and Al are homogeneously distributed on the silica support. Unfortunately the metal Nps size is too small to provide a definite composition by electron microscopy or X-ray diffraction, yet reasonable hypotheses can be drawn. Al^{3+} sites are hardly reduced and are highly oxophilic, typically forming robust bonds with silica supports.¹⁸ This was confirmed by X-ray photoelectron (XPS) analysis, which shows that the Al 2p peak position remains fixed at 74.6 eV both before and after the thermal treatment under H_2 and is consistent with Al^{3+} (see SI).¹⁹ In contrast, iridium can be easily reduced under hydrogen atmosphere to form Ir(0) Nps.^{20,21} In fact, the reduction of Ir in **2-s** can easily be followed in the Ir 4f_{7/2} XPS spectra. Initially, **2-s** displays an Ir 4f_{7/2} binding energy (B.E.) of 61.7 eV, which is in line with an Ir^{3+} complex containing electron-rich ligands such as Cp^* .²² After H_2 treatment, the formation of Ir(0) is confirmed by the appearance of a second pair of peaks with a lower Ir 4f_{7/2} B.E. of 60.6 eV. We thus propose that the **Ir-Al/SiO₂** material features small Ir(0) Nps surrounded by a high density of Al^{3+}

sites located at the Nps/support interface. Similar situation was described by Copéret and coworkers, who generated Cu Nps on silica containing Zr(IV)²³ or Ti(IV)²⁴ isolated sites. Still, the partial incorporation of Al atoms into the metal Nps cannot be ruled out.

In parallel, we prepared a monometallic iridium analogous material to serve as benchmark for catalysis. The sample was prepared using incipient wetness impregnation (IWI), by the addition of an appropriate volume (340 μL) of a 1.24M THF solution of Cp^*IrH_4 onto 295 mg of SBA-15₇₀₀ to reach a similar iridium loading than that obtained in the **Ir-Al/SiO₂** material, and the solvent was further evacuated under vacuum at room temperature. We reported before that Cp^*IrH_4 does not react with silica surface silanols,¹⁴ and is physisorbed at the surface of the support, which is notably confirmed by the $\nu(\text{Ir-H})$ signature in this material (Figure 1-d) which is identical to that of the IrCp^*H_4 precursor²⁵ ($\sigma=2150\text{ cm}^{-1}$). We then reduced this material under the same conditions (1 bar H_2 , 250°C) used for the aluminium-iridium catalyst, to yield material **Ir/SiO₂** as a dark brown powder (Scheme 1, bottom). The elimination of the Cp^* ligands during such treatment is confirmed by the disappearance of the $\nu(\text{C-H})$ signals around 2950 cm^{-1} (Figure 1-e). A strong shift of the $\nu(\text{Ir-H})$ band from 2150 to 2024 cm^{-1} is observed on the IR spectrum of **Ir/SiO₂**. This signature is very similar to that of **Ir-Al/SiO₂** (Figure 1-c). This suggests that the Nps resulting from the decomposition of physisorbed Cp^*IrH_4 have similar hydride sites than those resulting from the decomposition of species **2-s**, which is in favour of the formation of monometallic Ir(0) Nps in both cases. STEM analyses of **Ir/SiO₂** reveal the presence of small Ir Nps at the surface of the SBA-15₇₀₀ support (see Figure 2B and ESI). The Nps size distribution of **Ir/SiO₂** is the same to that of **Ir-Al/SiO₂** with a mean size of $1.6\pm 0.4\text{ nm}$. A few Ir aggregates (3-15 nm) were also noticed in some silica grains by STEM (see ESI). The Ir $4f_{7/2}$ XPS spectra (see ESI) clearly show the decrease of the Ir^{3+} peak at 61.6 eV and the appearance of the Ir(0) peak at 60.1 eV after the reduction step. Although the B.E. is low for metallic Ir, this is quite consistent with the reduced average coordination number of surface atoms found in Nps.²⁶ A small contribution of an Ir^{3+} peak is still present after H_2 treatment for both **Ir/SiO₂** and **Ir-Al/SiO₂**, corresponding to a $\text{Ir}(0):\text{Ir}^{3+}$ ratio of ca. 3:1 (see Figure 3 and ESI). This is either due to incomplete reduction or to the presence of Ir(III) hydride sites at the surface of the Nps.

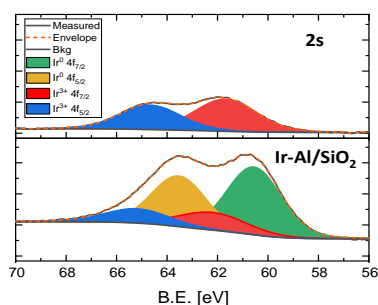
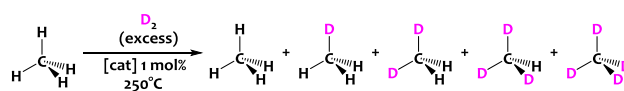


Figure 3 – XPS Ir 4f spectra of materials **2-s** (top) and **Ir-Al/SiO₂** (bottom).

Importantly, H_2 chemisorption studies on **Ir-Al/SiO₂** and **Ir/SiO₂** showed similar Ir dispersions of 67% and 56% respectively. This corresponds to a Np average diameter of 1.4 nm and 1.7 nm respectively using a truncated cubic octahedron geometry (see ESI), which is in good agreement with the STEM analyses, and indicates a comparable amount of accessible surface metal atoms for both catalysts.

To evaluate the potential of these new materials in catalysis we studied the hydrogen/deuterium isotope exchange (HIE) reaction between CH_4 and D_2 (Scheme 2). The reaction was carried out in a batch reactor at 250°C. The **Ir-Al/SiO₂** (1.0 mol% ± 0.1 mol% Ir compared to methane) and **Ir/SiO₂** (1.2 mol% ± 0.1 mol%) catalysts were exposed to a mixture of dry CH_4 (42 mbars) and dry D_2 (980 mbars) such as the D/H atomic ratio in the gas phase is ca 12. The catalyst loading of **Ir/SiO₂** is slightly higher than that of **Ir-Al/SiO₂** to compensate the small dispersion difference, and achieve a similar Ir surface sites quantity for both catalysts (0.67 mol% ± 0.03 mol%).



Scheme 2 – Deuteration of methane (42 mbars) into $\text{CH}_{4-x}\text{D}_x$ isotopomers at $T=250^\circ\text{C}$ using D_2 gas (980 mbars) as a deuterium source.

In the course of the reaction, methane isotopomers – noted $\text{CH}_{4-x}\text{D}_x$ (x being from 0 to 4) – are produced and quantified by GC-MS. The precise amount of each isotopomer was determined as a function of methane conversion (Figure 4) according to the fragmentation models given by Dibeler and Mohler.²⁷ To consolidate these results, the isotopic distribution was also determined by a complementary mathematical approach developed by Schoofs and his team.²⁸ From these data, it is possible to calculate the deuteration rate of methane – noted τ thereafter – by using the following relation: $\tau = 0.25\text{CH}_3\text{D} + 0.5\text{CH}_2\text{D}_2 + 0.75\text{CHD}_3 + \text{CD}_4$. Note that since $\text{D}/\text{H}\approx 12$ in our case, the thermodynamic equilibrium – noted τ_{eq} – of the reaction is reached for a deuteration rate of 92%.

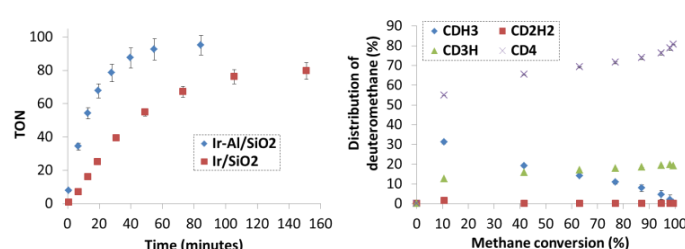


Figure 4 – Monitoring catalytic H/D exchange of methane. Left: Turnover number as a function of reaction time for catalysts **Ir-Al/SiO₂** (blue diamonds) and **Ir/SiO₂** (red squares) at 250°C and 0.67 mol% Ir surface sites. Right: distribution of deuteromethanes as a function of CH_4 conversion for **Ir-Al/SiO₂**. All the data were extracted by averaging Dibeler-Mohler²⁷ and Schoofs²⁸ calculations. Error bars account for uncertainty on catalyst loading and on the standard deviation between Dibeler-Mohler and Schoofs calculations. The catalysts turnover numbers are calculated as follow: $\text{TON} = \tau \cdot n_{\text{CH}_4}/n_{\text{Ir}}$, where n_{Ir} is the total number of moles of iridium in the catalyst.

Comparative TONs for both catalysts are plotted on Figure 4-left. The **Ir-Al/SiO₂** catalyst is more active and operates the H/D exchange of methane at a maximum turnover frequency (TOF) of 339 h^{-1} versus 117 h^{-1} for **Ir/SiO₂**. Note that similar

trends are obtained when turnover numbers are corrected from the Ir dispersion extracted from the H₂ chemisorption studies (Figure S25). Furthermore, 50% deuterium incorporation into methane is observed after 12 minutes for Ir-Al/SiO₂ versus 34 minutes for Ir/SiO₂ and the thermodynamic equilibrium is reached within 65 minutes for Ir-Al/SiO₂ versus 145 minutes for Ir/SiO₂. These kinetic data testify to the higher catalytic activity of the aluminium-iridium catalyst with respect to its monometallic iridium counterpart by a factor of about three, which is not negligible. Note that this kinetic behaviour was reproduced on independently synthesized samples. Importantly, the spent Ir-Al/SiO₂ and Ir/SiO₂ catalysts were exposed to air and then re-used in catalysis, and identical performances were obtained in this second catalytic run (Fig. S26 and S27), highlighting the good robustness of these materials. STEM analyses of the spent catalyst show no modification of the particles size distribution. Decreasing the catalyst loading to 0.1 mol% resulted in an increased TON of 900 after 9 hours, without evidence of catalyst deactivation. **2-s** was also tested in catalysis, and was active only after a prolonged induction period of several hours, corresponding to the removal of the Cp* ligands and the *in-situ* formation of Nps (Figure S23).

To get insights into the mechanisms in place here between the gas phase (CH_{4-x}D_x and D₂) and the surface of the catalysts, we paid attention to the distribution of deuteromethane isotopomers as a function of methane conversion rate (Figure 4, right). For both catalysts, similar selectivity is observed (see ESI). CD₄ is the major isotopomer at low CH₄ conversion (10 to 20%), but a subsequent amount of CH₃D is also observed. Then, the relative amount of CD₄ increases while the CH₃D proportion drops as CH₄ is consumed. Interestingly, the amount of CH₂D₂ stays negligible in the reactional medium (<2%) whatever the CH₄ conversion. Two main mechanisms are known for methane H/D exchange: (i) stepwise exchange, in which CDH₃ is the major product at low conversion with negligible amount of CD₄, and (ii) multiple exchange, in which the C–H activations subsequent to adsorption are faster than the desorption step, which gives CD₄ as major product at low CH₄ conversion (see ESI for details).^{1–3} In the present case, the data suggest an important contribution of a multiple exchange mechanism, in which the rate determining step is the CH₄ dissociative adsorption step, which may be facilitated by the presence of the Al³⁺ sites at the direct proximity of the Ir particles.

In summary, a SOMC synthetic methodology is used to generate the surface species (≡SiO)Al(Cp*IrH₃)₂, **2-s**, ensuring a good dispersion of both metallic components (Al & Ir) on the silica support. Thermal hydrogenolysis of **2-s** leads to the formation of small (<2 nm), narrowly distributed Ir Nps surrounded by a high density of Al³⁺ sites located at the Nps/silica support interface. This Ir-Al/SiO₂ catalyst demonstrated enhanced catalytic performances in the H/D exchange of methane in comparison with the monometallic Ir/SiO₂ analogue, highlighting the promoting effect of aluminium. Although H/D exchange in methane has been studied with a large number of transition metal catalysts,³ the

promoting effect of a Lewis acidic metal has not been described to the best of our knowledge. Both Ir-Al/SiO₂ and Ir/SiO₂ catalysts are air-stable and do not deactivate (at least down to 0.1 mol%), which is a clear advantage compared to silica-supported molecular metal hydrides, which are highly active in methane deuteration, but extremely air sensitive and deactivate easily.²⁹ This research was performed in the frame of a project funded by the French National Research Agency (ANR) (grant number ANR-21-CE07-0009-01 (SHICC)). There are no conflicts to declare.

Notes and references

- 1 C. Kemball, *Proc. R. Soc. London. Ser. A. Math. Phys. Sci.*, 1953, **217**, 376–389.
- 2 A. Frennet, *Catal. Rev.*, 1974, **10**, 37–68.
- 3 A. Sattler, *ACS Catal.*, 2018, **8**, 2296–2312.
- 4 P. J. Robertson, M. S. Scurrill and C. Kemball, *J. Chem. Soc. Faraday Trans. 1 Phys. Chem. Condens. Phases*, 1975, **71**, 903–912.
- 5 J. Joubert, A. Salameh, V. Krakoviack, F. Delbecq, P. Sautet, C. Copéret and J. M. Basset, *J. Phys. Chem. B*, 2006, **110**, 23944–23950.
- 6 C. Copéret, A. Comas-Vives, M. P. Conley, D. P. Estes, A. Fedorov, V. Mougel, H. Nagae, F. Núñez-Zarur and P. A. Zhizhko, *Chem. Rev.*, 2016, **116**, 323–421.
- 7 C. Copéret, *Acc. Chem. Res.*, 2019, **52**, 1697–1708.
- 8 S. R. Docherty, N. Phongprueksathat, E. Lam, G. Noh, O. V. Safonova, A. Urakawa and C. Coperet, *JACS Au*, 2021, jacsau.1c00021.
- 9 E. Lam, G. Noh, K. W. Chan, K. Larmier, D. Lebedev, K. Searles, P. Wolf, O. V. Safonova and C. Copéret, *Chem. Sci.*, 2020, **11**, 7593–7598.
- 10 E. Lam, G. Noh, K. Larmier, O. V. Safonova and C. Copéret, *J. Catal.*, 2021, **394**, 266–272.
- 11 J. Camacho-Bunquin, M. S. Ferrandon, H. Sohn, A. J. Kropf, C. Yang, J. Wen, R. A. Hackler, C. Liu, G. Celik, C. L. Marshall, P. C. Stair and M. Delferro, *ACS Catal.*, 2018, **8**, 10058–10063.
- 12 K. Searles, K. W. Chan, J. A. Mendes Burak, D. Zemlyanov, O. Safonova and C. Copéret, *J. Am. Chem. Soc.*, 2018, **140**, 11674–11679.
- 13 S. Lassalle, R. Jabbour, P. Schiltz, P. Berruyer, T. K. Todorova, L. Veyre, D. Gajan, A. Lesage, C. Thieuleux and C. Camp, *J. Am. Chem. Soc.*, 2019, **141**, 19321–19335.
- 14 S. Lassalle, R. Jabbour, I. Del Rosal, L. Maron, E. Fonda, L. Veyre, D. Gajan, A. Lesage, C. Thieuleux and C. Camp, *J. Catal.*, 2020, **392**, 287–301.
- 15 I. Del Rosal, S. Lassalle, C. Dinoi, C. Thieuleux, L. Maron and C. Camp, *Dalton Trans.*, 2021, **50**, 504–510.
- 16 L. Escomel, N. Soulé, E. Robin, I. Del Rosal, L. Maron, E. Jeanneau, C. Thieuleux and C. Camp, *Inorg. Chem.*, 2022, acs.inorgchem.1c03120.
- 17 L. Escomel, I. Del Rosal, L. Maron, E. Jeanneau, L. Veyre, C. Thieuleux and C. Camp, *J. Am. Chem. Soc.*, 2021, **143**, 4844–4856.
- 18 I. B. Moroz, P. Florian, J. Viger-Gravel, C. P. Gordon, A. Lesage and C. Copéret, *Angew. Chemie - Int. Ed.*, 2020, anie.202006285.
- 19 J. Moulder and J. Chastain, *Handbook of x-ray photoelectron spectroscopy: a reference book of standard spectra for identification and interpretation of XPS data*, 1992.
- 20 F. Héroguel, G. Siddiqi, M. D. Detwiler, D. Y. Zemlyanov, O. V. Safonova and C. Copéret, *J. Catal.*, 2015, **321**, 81–89.
- 21 F. Héroguel, D. Gebert, M. D. Detwiler, D. Y. Zemlyanov, D. Baudouin and C. Copéret, *J. Catal.*, 2014, **316**, 260–269.
- 22 B. Van Dijk, G. M. Rodriguez, L. Wu, J. P. Hofmann, A. MacChioni and D. G. H. Hetterscheid, *ACS Catal.*, 2020, **10**, 4398–4410.
- 23 E. Lam, K. Larmier, P. Wolf, S. Tada, O. V. Safonova and C. Copéret, *J. Am. Chem. Soc.*, 2018, **140**, 10530–10535.

- 24 G. Noh, E. Lam, J. L. Alfke, K. Larmier, K. Searles, P. Wolf and C. Copéret, *ChemSusChem*, 2019, **12**, 968–972.
- 25 T. M. Gilbert, F. J. Hollander and R. G. Bergman, *J. Am. Chem. Soc.*, 1985, **107**, 3508–3516.
- 26 J. Radnik, C. Mohr and P. Claus, *Phys. Chem. Chem. Phys.*, 2003, **5**, 172–177.
- 27 F. L. Mohler, V. H. Dibeler and E. Quinn, *J. Res. Natl. Bur. Stand. (1934)*, 1958, **61**, 171.
- 28 B. Schoofs, J. A. Martens, P. A. Jacobs and R. A. Schoonheydt, *J. Catal.*, 1999, **183**, 355–367.
- 29 G. L. Casty, M. G. Matturro, G. R. Myers, R. P. Reynolds and R. B. Hall, *Organometallics*, 2001, **20**, 2246–2249.